NUREG-0288

MODELING OF POOL SWELL DYNAMICS

Progress Report
March 1977

Massachusetts Institute of Technology
for
U. S. Nuclear Regulatory Commission

Available from
National Technical Information Service
Springfield, Virginia 22161
Price: Printed Copy $4.00 ; Microfiche $3.00

The price of this document for requestors outside of the North American Continent can be obtained from the National Technical Information Service.

NUREG-0288
NRC-4

MODELING OF POOL SWELL DYNAMICS

Progress Report
March 1977

W. G. Anderson
P. W. Huber
A. A. Sonin

Manuscript Completed: March 1977
Date Published: June 1977

Department of Mechanical Engineering
Massachusetts Institute of Technology
Cambridge, MA 02139

Prepared for
Division of Reactor Safety Research
Office of Nuclear Regulatory Research
U. S. Nuclear Regulatory Commission
Under Contract No. NRC-04-77-011

SUMMARY

(1) Three geometrically similar, drum-shaped, single-downcomer wetwell test sections have been constructed, with diameters of 14 cm, 28 cm, and 54 cm, respectively.

(2) Three series of tests have been completed in the medium-size system (28 cm dia.), using water as the liquid and air, argon, and helium as blowdown gases. A broad range of operating conditions was covered in each test series, roughly representative of Mark I conditions. A comparison of the tests with argon and helium, whose enthalpies differ by a factor of 10 at the same temperature, clearly shows that proper pool swell scaling is obtained only if the enthalpy flux through the downcomer is adjusted according to Moody's scaling law.

(3) One series of tests has been completed in the small system (14 cm dia.), using water as the liquid and air as the gas. Comparison of these results with the corresponding ones obtained with the medium-size system again favors Moody's scaling law for pool swell phenomena.

(4) The peak downward pressure on the model containment system floor, which occurs just after vent clearing, i.e., before significant perturbation of the pool surface, appears to be affected by fluid-structure interactions. These interactions do not, however, influence pool swell and the loads after vent clearing.

1. INTRODUCTION

The purpose of this research program, which was funded 1 October 1976, is to develop and verify the scaling laws which apply to LOCA-induced pool swell in BWR pressure-suppression containment systems. The work has now progressed to a stage where several critical series of experiments have been completed, and we are in a position to give a preliminary report on our findings.

In Section 2 of this report, we summarize the present understanding of the scaling laws for pool swell. Our experimental test program for checking the scaling laws is outlined in Section 3. Section 4 describes some of the experimental results we have obtained to date, and Section 5 summarizes the conclusions we can draw from them.

2. THE DYNAMIC SCALING LAWS

2.1 Moody's Scaling Laws

A set of modeling parameters and scaling laws for the general pool dynamics problem has been derived by F. Moody of G.E. [1]. The scaling laws are based first of all on the hypothesis that once the air bubble forms after the fluid slug is ejected from the inside of the downcomer, the bubble can be viewed as a constant-pressure region of non-condensable gas, driven by an enthalpy flux from the exit of the downcomer and resisted by the inertia of the water above it as

well as by the compliance of the air space above the water. In addition, it is argued that heat transfer from bubble air to the water is negligible, and that viscous losses in the bubble and in the pool water are also negligible. Surface tension effects are not accounted for, so that the scaling laws do not apply to any smaller-scale fluid breakup which may occur as the bubble breaks the surface of the pool (the maximum loads occur prior to this time, however).

Apart from the requirement that the model and full-scale system be completely similar geometrically, dynamic similarity of the (pre-breakthrough) pool swell dynamics also requires that the following two dimensionless quantities have the same values in the model and full-scale system:

$$\pi_1 = \gamma \tag{1}$$

$$\pi_2 = \frac{P_i}{\rho g D} \quad , \tag{2}$$

and that two additional dimensionless variables

$$\pi_3 = \frac{P_0}{P_i} \tag{3}$$

$$\pi_4' = \frac{G h_0}{\rho g^{3/2} D^{3/2}} \tag{4}$$

have the same value in the model and full-scale systems at corresponding values of the dimensionless time

$$t^* \equiv t \sqrt{g/D} \quad . \tag{5}$$

Here,

γ = specific heat ratio c_p/c_v ;

P_i = initial pressure in the wetwell trapped air sp ;

ρ = pool liquid density;

g = acceleration of gravity;

D = a dimension identifying scale of system in the general case; in our case, the wetwell diameter;

P_0 = drywell air pressure (function of time);

G = air mass flow rate through downcomer per unit area (function of time);

h_0 = stagnation enthalpy of air in drywell (function of time);

t = time from initiation of LOCA; in our case, time from valve opening.

We shall call the quantities π_1, π_2, $\pi_3(t^*)$, and $\pi_4'(t^*)$ the modeling parameters. The modeling parameters are a set of independent dimensionless variables which, once specified, uniquely determine the pool swell dynamics in dimensionless terms.

For any dependent variable like a particular local pressure p, one can define a dimensionless form like

$$p^* = \frac{p - P_i}{P_0} \quad , \tag{6}$$

which, according to the laws of dimensional analysis, is a function only of t^*, π_1, π_2, π_3 and π_4'. Thus,

$$p^* = p^*\left[t^*, \pi_1, \pi_2, \pi_3(t^*), \pi_4'(t^*)\right] \quad . \tag{7}$$

The general modeling procedure is this: one chooses conditions in the scale model tests such that the four modeling parameters π_1 to π_4' have the same values as in the full-scale system (in the case of π_3 and π_4', the values must be the same at all values of the dimensionless time t*). This ensures that the values of the dimensionless dependent variables like p^* are the same in the model as in the full-scale system, at corresponding t^*. Having measured p^* versus t^* in the model, one can then predict P versus t in the full-scale system, using Eq. (6). Relations like Eq. (6) can be called the scaling laws for the dependent variables, since they tell us how a dependent variable measured in a small-scale simulation can be scaled up to the full-scale system.

2.2 Moody's Scaling Laws in Modified Form, for Orificed Downcomers

The difficulty with applying Moody's scaling laws to small-scale modeling is that the absolute pressures and the enthalpy flux density Gh_0 have to be independently adjusted with scale, the former in proportion to ρD and the latter to $\rho D^{3/2}$, over the whole blowdown time span.

Now, the enthalpy flux in a model can be adjusted independently of pressure by the insertion of a flow-control orifice inside the downcomer (Fig. 1). The question then arises, what are the criteria for when an orifice will accurately simulate the enthalpy flux during the entire blowdowm, assuming that the model drywell pressure is properly simulated?

We have answered this question by considering the scaling laws for the flow through an orifice in a pipe. Consider a number of geometrically similar pipes (Fig. 1) with the same length-to-diameter ratios, and similar orifices of diameter d_i placed at geometrically similar places in the pipes. From dimensional considerations we can show that a dimensionless mass flux density, which we shall call the mass flow coefficient C_m, in analogy to the discharge coefficient C_d for volume flow in nozzles,*

$$C_m \equiv \frac{G}{\rho_0 \left[\frac{2(P_0 - P)}{\rho_0}\right]^{\frac{1}{2}}} \tag{8}$$

must have the functional form

$$C_m = C_m\left(\frac{d_i}{d}, \frac{P_0-P}{P_0}, \gamma, Re\right) \tag{9}$$

where $G \equiv$ gas mass flow per unit area through the downcomer;

$\rho_0 \equiv$ gas density in the drywell;

$P_0 \equiv$ drywell pressure;

$P \equiv$ pressure at exit of downcomer;

$d_i \equiv$ orifice diameter;

---

*Note that in the incompressible flow limit $(P_0-P)/P \to 0$, the mass flow coefficient is related to the usual head loss coefficient k, or fL/D, based on exit speed and ρ_0, according to

$$C_m = \frac{1}{\sqrt{1 + k}} \quad .$$

and

$$\mathrm{Re} \equiv \frac{\sqrt{\rho_0 P_0}\, d}{\mu_0} = \frac{P_0 d}{\mu_0 \sqrt{RT_0}} \tag{10}$$

is a characteristic Reynolds number for the flow, with

μ_0 = viscosity of gas in drywell;

T_0 = drywell gas temperature;

R = specific gas constant for the gas (universal gas constant divided by molar mass).

Now, in terms of the newly introduced mass flow coefficient, Moody's enthalpy flux scaling parameter π_4' can be written as

$$\pi_4' = \frac{Gh_0}{\rho g^{3/2} D^{3/2}} = \sqrt{2}\, \frac{\gamma}{\gamma-1} \frac{P_i}{\rho g D} \frac{P_0}{P_i} \left(\frac{P_0-P}{P_0}\right)^{1/2} \left(\frac{RT_0}{gD}\right)^{1/2} C_m \tag{11}$$

$$= \sqrt{2} \left(\frac{\pi_1}{\pi_1-1}\right) \pi_2\, \pi_3 \left(1 - \frac{1}{\pi_3} - p^*\right)^{1/2} \left(\frac{RT_0}{gD}\right)^{1/2} C_m \ .$$

Now if dynamic similarity is achieved, π_1. π_2, π_3, and p^* will automatically be identical in the model and the reference ("full-scale") system, as we have seen in the previous section. It follows, then, that π_4' will be the same in the model as in the reference system if $\sqrt{RT_0/gD}\, C_m$ is the same at corresponding values of t^*, or according to Eq. (9), at corresponding values of $(P_0-P)/P_0$. Thus, we can replace the scaling law expressed by Eq. (4) by the requirement that

$$\pi_4 \equiv \left(\frac{RT_0}{gD}\right)^{1/2} C_m \tag{12}$$

must have the same value in the model and reference system at corresponding pressure ratios $(P_0-P)/P$. If this requirement is satisfied then the enthalpy flux scaling parameter expressed earlier by π_4' will automatically be properly modeled if π_1, π_2, and π_3 are properly modeled.

Our conclusion, then, is that the proper modeling laws for pool swell are that

$$\pi_1 \equiv \gamma \tag{13}$$

and

$$\pi_2 = \frac{P_i}{\rho g D} \tag{14}$$

be the same in the model and reference system, that

$$\pi_3 = \frac{P_0}{P_i} \tag{15}$$

be the same in the model and reference system at corresponding values of $t^* \equiv t\sqrt{g/D}$, and that

$$\pi_4 \equiv \left(\frac{RT_0}{gD}\right)^{\frac{1}{2}} C_m \tag{16}$$

be the same for the (orificed) model downcomer as for the reference system at all values of the dimensionless pressure drop $(P_0-P)/P_0$ encountered in the process. A dimensionless dependent variable like the pressure p^* defined earlier will have the form

$$p^* = p^*\left[t^*, \pi_1, \pi_2, \pi_3(t^*), \pi_4\left(\frac{P_0-P}{P_0}\right)\right] \quad ; \tag{17}$$

that is, the value of p^* for the reference system will be the same

as for the model if the modeling parameters π_1 to π_4 are the same in both.

The adjustment of π_4 in the model to that of the reference (or full-scale) system is made by choosing a suitable orifice diameter d_i [see Eq. (9)]. This can be done after several orifices with different d_i's have been calibrated at their design Re's [see Eq. (10)] over the range of $(P_0-P)/P$ expected in the blowdown process.

3. EXPERIMENTAL PROGRAM

The scaling laws are being verified experimentally by studying the pool swell problem on a small-scale in the somewhat simplified "containment system" geometry shown in Fig. 2. The "wetwell" is a simple cylindrical vessel of internal diameter D and height $2.18D$. A single downcomer with internal diameter $d = 0.182\ D$ enters the wetwell from the top center. The downcomer length is 15 diameters, that is, $2.73\ D$. The top of the downcomer opens directly into a "drywell," which in our case is simply a reservoir with a volume large compared with that of the airspace in the wetwell, so that the drywell pressure remains essentially constant during the entire blowdown process.

Under design conditions, the wetwell is precisely half full of water, and the downcomer submergence is $2d$ or $0.264\ D$. Both water level and submergence can, however, be independently varied.

Although our system is not intended to be geometrically identical

to any particular existing containment system, its gross geometric parameters (see Table 1) do roughly simulate the GE Mark I system.

The gas flow rate through the downcomer can be independently controlled in our system by placing interchangeable orifice plates (Fig. 1) in the downcomer 11.5 diameters (i.e., 2.1 D) upstream of the downcomer exit.

A pneumatically operated, fully-opening valve (essentially, a rubber-lined flat disc which, when closed, is pressed against the top lip of the downcomer, and when opened simply lifts away from it) starts the blowdown. The valve opening time is short and does not affect the flow processes which ensue.

Our intention is to verify the scaling laws by setting the scaling parameters at certain chosen fixed values, but independently varying the quantities P_i , P_o, ρ, D, R, and C_m which make up the scaling parameters, and checking whether the dimensionless dependent variables like pressure p^* indeed do remain invariant, as predicted by the scaling laws. The test sections are instrumented to measure pressure (via Kistler Model 206 low-pressure Piezotron transducers) in four places, as shown in Fig. 2.

Table 2 shows the values which the scaling parameters are given in our tests. Also shown for reference are the corresponding values for a design basis LOCA in a Mark I GE containment system.

In our test program, the system size will be varied by a linear factor of 4 . We have completed construction of three test sections, with D = 14 cm, 28 cm, and 54 cm. These will be referred to as the

small, medium, and large systems, respectively. Each system has a series of orifices for the independent control of the enthalpy flux parameter π_4 through C_m [see Eq. (16)].

Three gases will be used: air (with $\gamma = 1.4$), and helium and argon (with $\gamma = 1.67$). The latter two are chosen because their gas constant $\bar{R}$ differs by a factor of 10, and hence allows the parameter π_4 to be changed by a factor of 3.16 by changing gas alone, without changing pressures, flow orifice, or system size.

Also, three liquids will be used: water, meriam fluid (specific gravity $\simeq$ 3) and, in the small and medium systems, mercury (specific gravity $\simeq$ 13.6).

The absolute pressures will be varied over a factor of 30 to keep the scaling parameters π_2 and π_3 constant while D and ρ are changed as described above.

The flow constriction diameter d_i/d relative to the downcomer diameter will be varied over a factor of 3 .

4. EXPERIMENTAL RESULTS OBTAINED TO DATE

4.1 General Remarks

At the present time, all three test sections (D = 14 cm, 28 cm, and 54 cm) have been constructed, and a considerable number of tests have been performed with the medium-size and the small-size systems. In the medium-size system, tests have been run with air, argon, and helium as the gas and water as the liquid. For each gas, the parameter $P_i/\rho gD$ was set at both 4.2 and 8.4, and P_0/P_i was given values 2, 2.5, and 3. Several orifices were used in each case, so that a range of values of the enthalpy flux parameter π_4 was covered for each gas.* In the small-size system, the tests to date have been confined to the air/water combination, but with the same values of $P_i/\rho gD$ and P_0/P_i, and again for several values of the enthalpy flux parameter.

Figure 3 shows some typical pressure histories, in this case measured in the medium-size system. The plots are traced directly from

---

*The calibration of each orifice for C_m as a function of $(P_0-P)/P_0$ is done by measuring the initial rate of pressure rise in the empty wetwell (i.e., no liquid) when the valve is opened. Using the first law of thermodynamics, and assuming adiabatic conditions, it is easy to show that

$$C_m\left(\frac{P_0 - P_i}{P_0}\right) = \frac{V}{\frac{\pi d^2}{4}\gamma\sqrt{2RT_0}}\left(\frac{P_0 - P_i}{P_0}\right)^{\frac{1}{2}}\frac{1}{\tau} \quad ,$$

where V is the total wetwell volume and τ is the time it would take the wetwell pressure to reach P_0 if it were to keep rising at its initial rate.

oscillograms. Trace (a) represents the pressures on the wetwell floor (center), and trace (b) the pressure on the wetwell ceiling. Trace (c) is the pressure at a point in the downcomer, just downstream of the orifice (see Fig. 2). (We use this trace mainly to establish t=0.)

The physical phenomena which give rise to these pressure histories can be described as follows. Valve opening is signaled by a rapid rate of pressure rise in the downcomer (Fig. 3c). The positive pressure in the downcomer begins to push the water in the downcomer downward. Initially, the pressure on the floor (Fig. 3a) responds with only a slight rise, since almost the entire increase in pressure is taken up across the slug of water in the downcomer, causing it to accelerate downward. However, as the air/water surface reaches the downcomer exit (the vent clears) and a bubble begins to form, the pressure in the downcomer is suddenly transmitted to the essentially stagnant water below it, and to the wetwell floor. The pressure difference is now taken up across the layer of water over the downcomer exit, and that layer begins to accelerate upward. Vent clearing thus gives rise to a very sudden, virtually step-function, increase in pressure on the wetwell floor (Fig. 3a), an increase from P_i to essentially the pressure inside the downcomer at the time of clearing (compare Figs. 3a and 3c). Actually, the floor pressure in this particular case overshoots the downcomer pressure, but the overshoot appears to result at least in part from vibrations set up in wetwell structure in response to the very suddenly applied load.

Structural oscillations give rise to pressure oscillations on the floor because they rapidly oscillate (accelerate) the water in

the wetwell and thereby induce pressure oscillations, below the water surface, much like the gravitational acceleration causes a pressure increase in the downward direction in water. The corresponding effect on the air pressures is negligible because the inertia of the air is a thousandfold less than that of water. More is said about the fluid-structure interactions in Section 4.3 below. In any case, the peak pressure on the floor, occurring just after vent clearing, does appear to be caused in part by a structural rebound and oscillations. The oscillations soon die out, however, and they do not affect the pressures in later parts of the blowdown process.

After the vent clears, the bubble begins to grow rapidly. The pressures in the downcomer and the wetwell floor decrease, roughly hand-in-hand, and the pressure on the ceiling begins to increase (Fig. 3b) as the airspace in the wetwell is compressed. The ceiling pressure reaches a maximum at the point of maximum compression of the airspace, at which point the airspace, which is overcompressed due to the inertia of the rising water, expands back towards a larger volume and the ceiling pressure drops. An increase in the floor and downcomer pressures occurs again since the bubble pressure is increasing. In the case shown, breakthrough occurs soon thereafter.

4.2 Some Experimental Results on the Pool Swell Scaling Laws

To make the checking of the scaling laws more convenient, we have selected five easily identifiable experimental quantities (dependent variables) for comparison between the various tests:

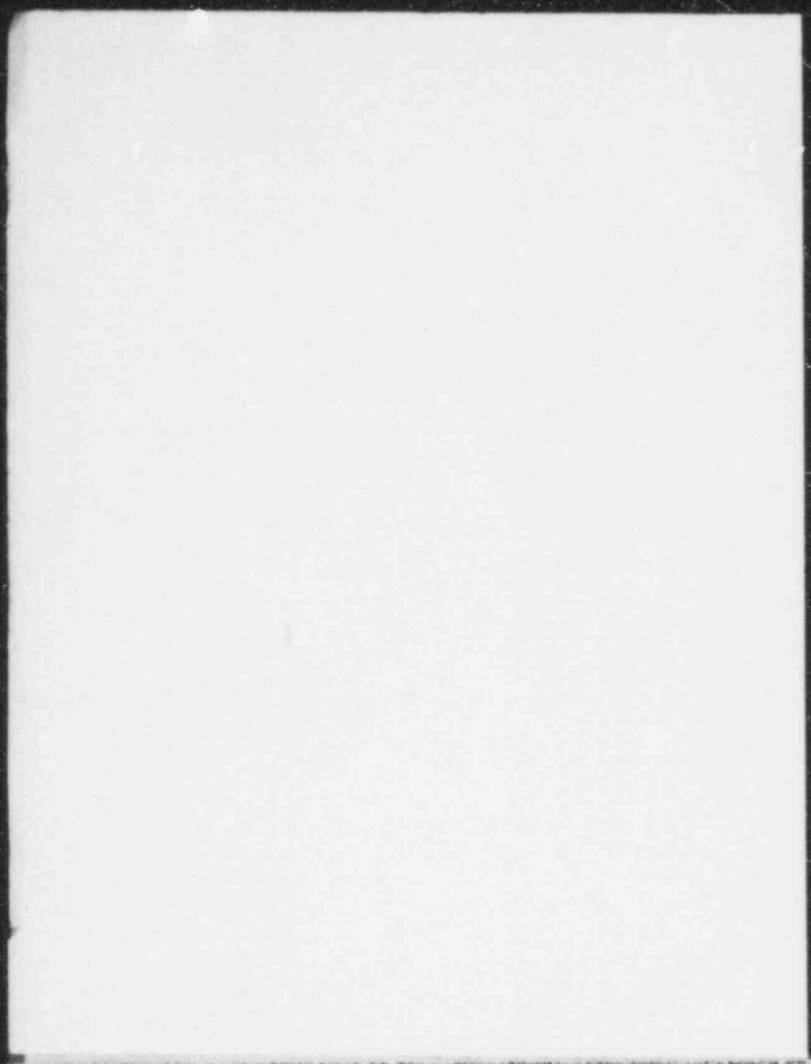
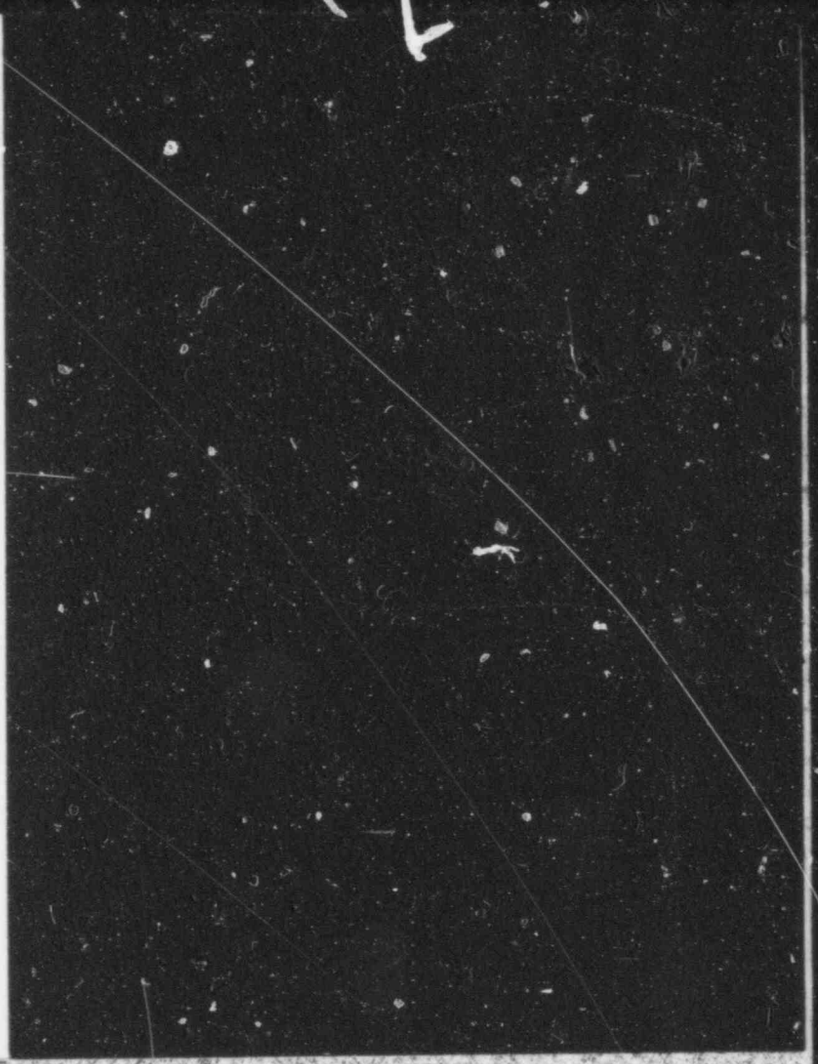
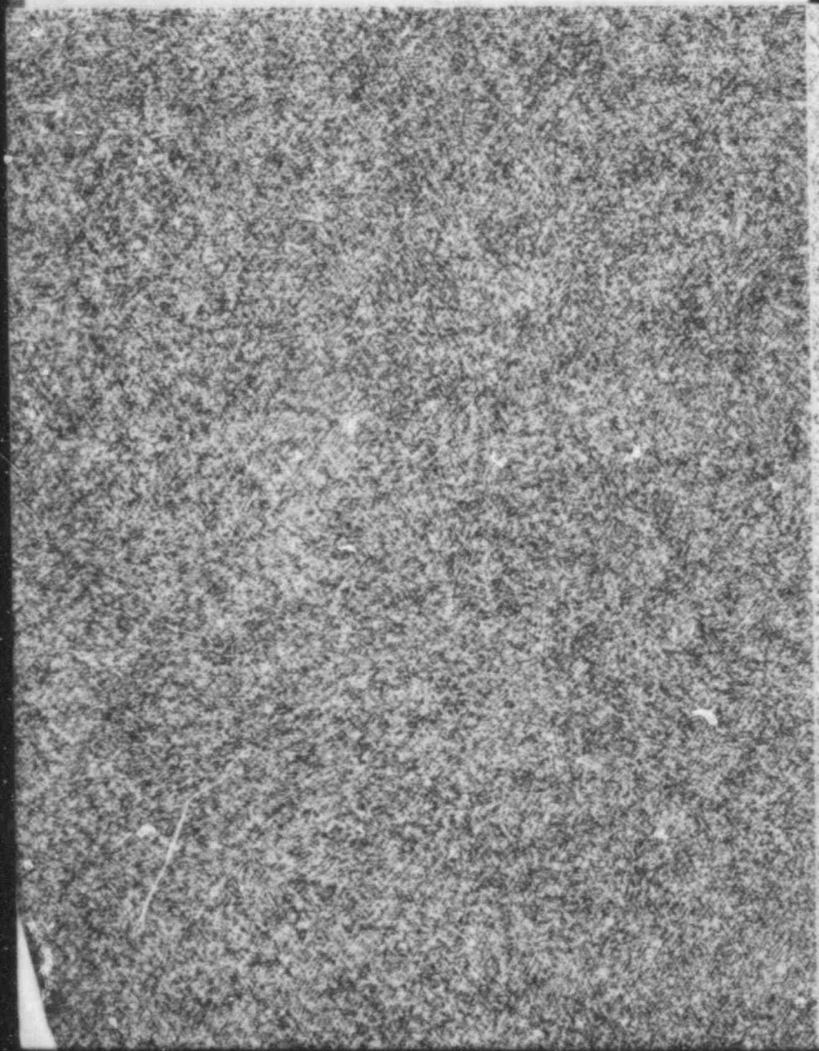


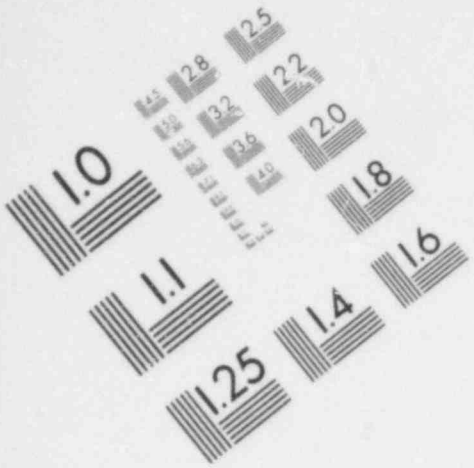

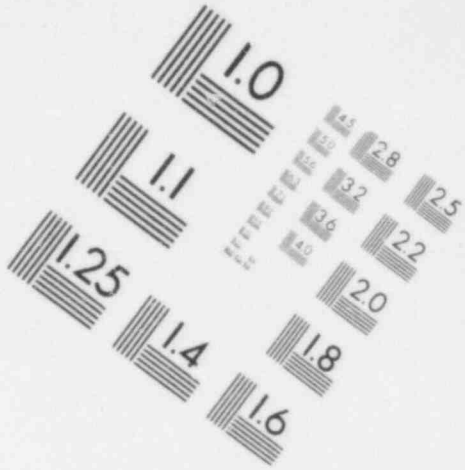

IMAGE EVALUATION
TEST TARGET (MT-3)

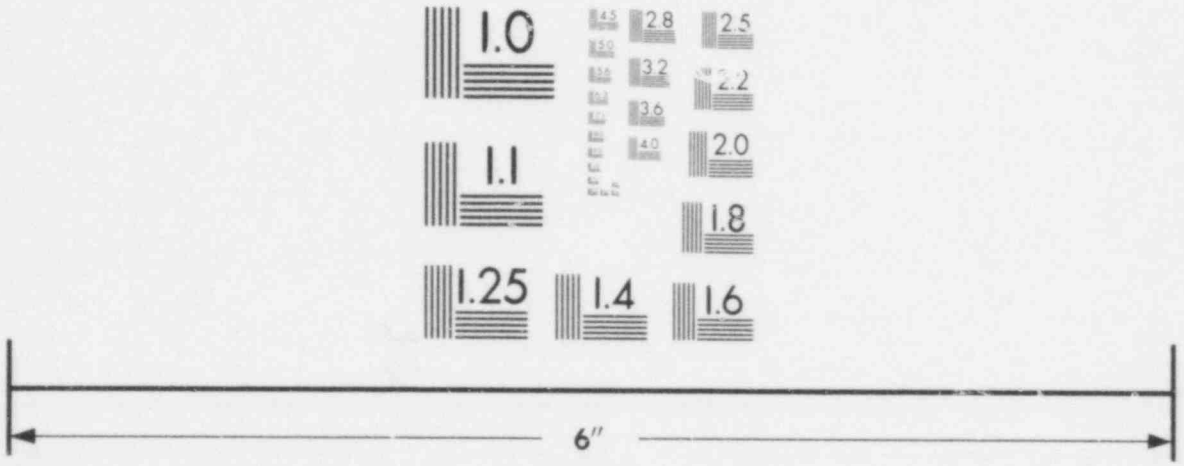

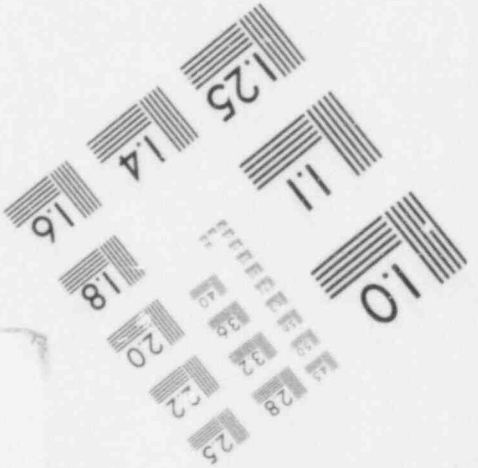

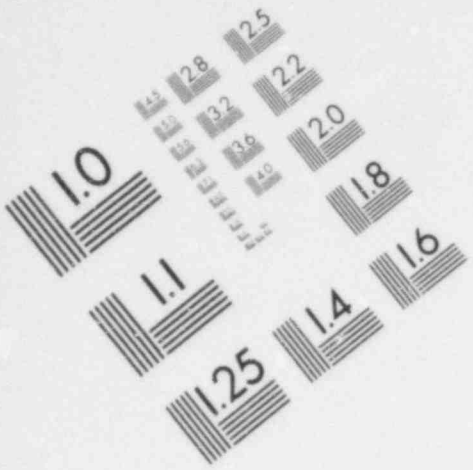

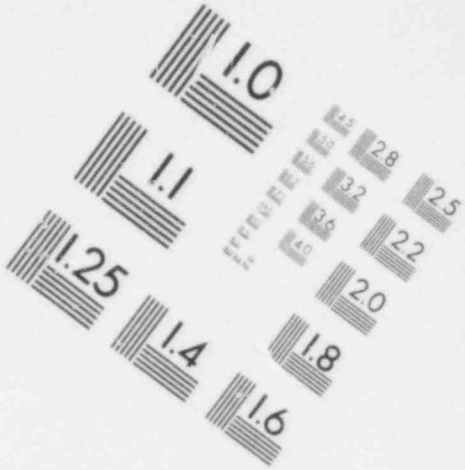

IMAGE EVALUATION
TEST TARGET (MT-3)

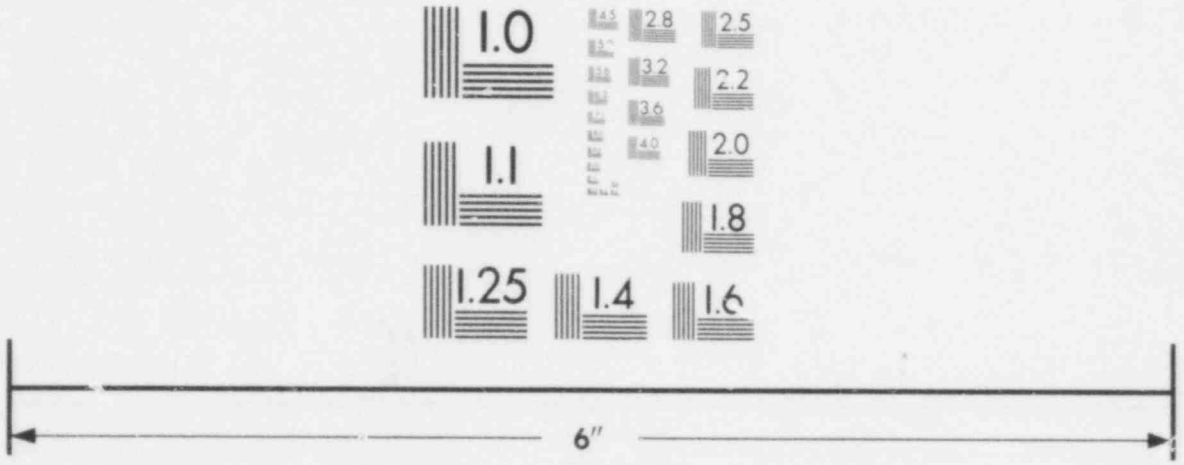

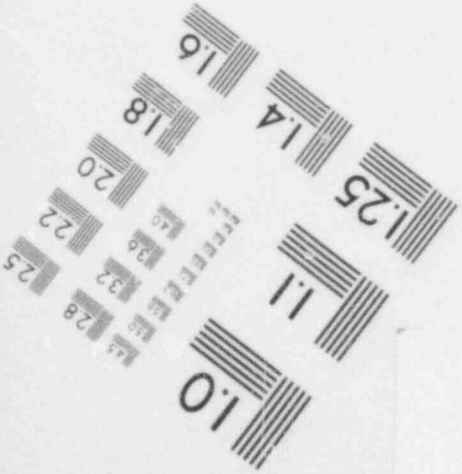

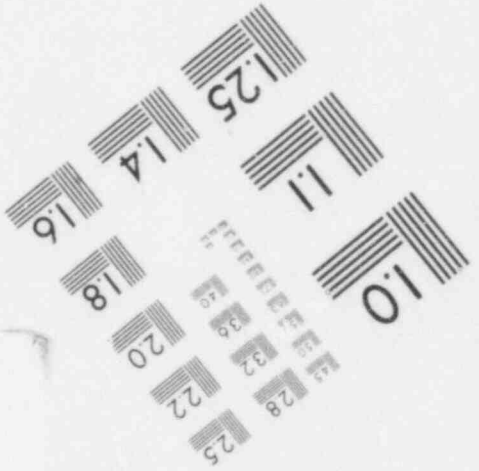

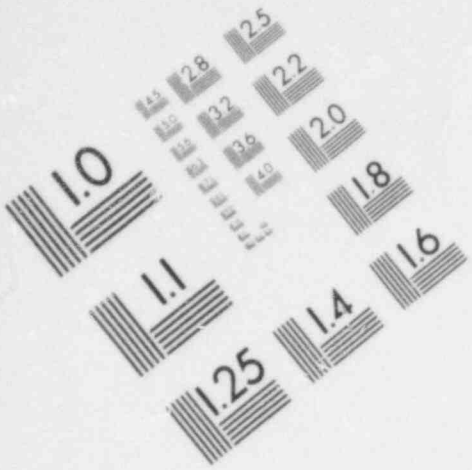

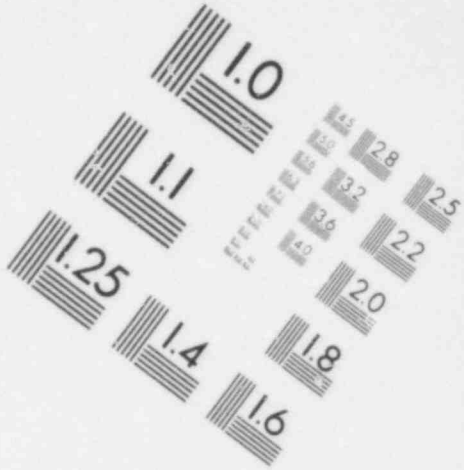

IMAGE EVALUATION
TEST TARGET (MT-3)

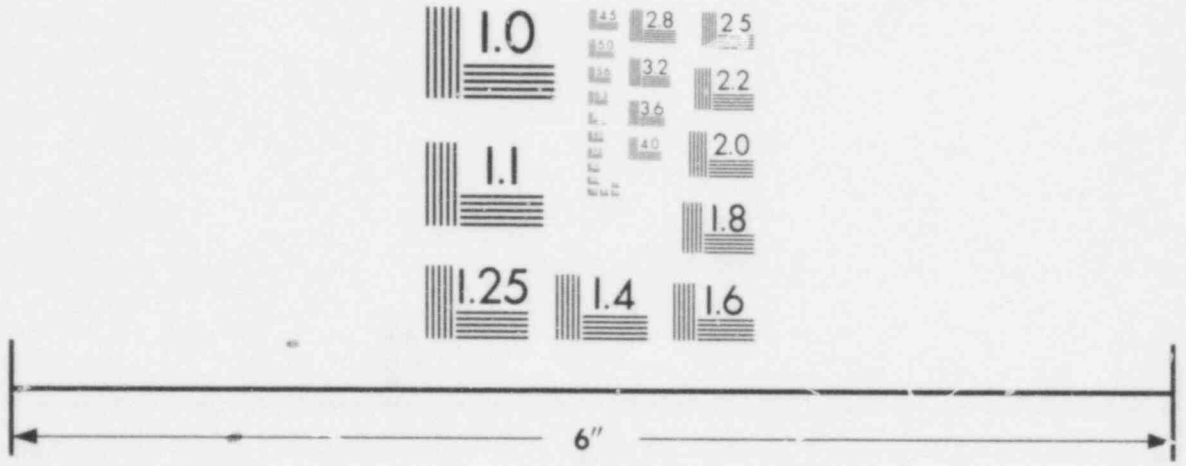

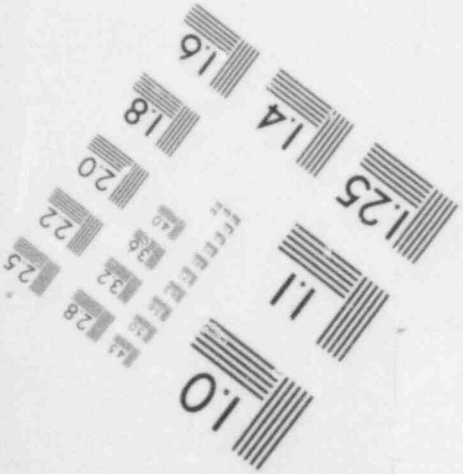

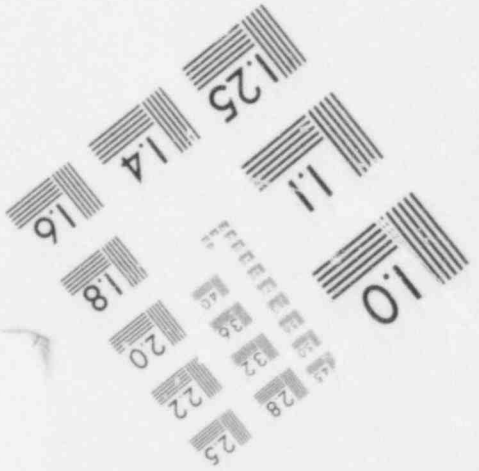

(1) the time of vent clearing;

(2) the minimum floor pressure after vent clearing (Fig. 3a);

(3) the time corresponding to the minimum floor pressure after vent clearing;

(4) the maximum ceiling pressure before breakthrough (Fig. 3b);

(5) the time corresponding to the maximum ceiling pressure before breakthrough.

The peak floor pressure associated with vent clearing is not used because it is affected by structural vibrations (Section 4.3), and these are not expected to scale according to Moody's laws, which were developed for pool swell in perfectly rigid containers.

We have made two types of fundamental checks on the scaling laws so far: (a) we have compared results obtained in a given size wetwell with two gases (helium and argon) which have vastly different enthalpies at the same temperature; and (b) we have compared results obtained with the same gas (air) in two different size systems.

The tests with helium and argon were carried out in the medium-size system (D = 28 cm), using water as the liquid in both cases. Orifices with various diameters d_i were used with both gases. Figure 4 shows the dimensionless form

$$p^* \equiv \frac{p - P_i}{P_0}$$

of the maximum ceiling pressure and the minimum floor pressure plotted versus the dimensionless diameter d_i/d of the orifice, for given values of $P_i/\rho gD$ and P_0/P_i. Clearly, for specified dimensionless driving pressures, and for a given system geometry and given internal

downcomer geometry (i.e., given d_i/d in this case), the different gases He and Ar produce vastly different dimensionless pressure loads. The difference is a factor of two in the ceiling pressure and as much as a factor of four in the floor pressure. The results shown are typical examples. Similar results were obtained with the other values of P_0/P_i and $P_i/\rho gD$.

Figure 5 shows the same data as Fig. 4, but now plotted as p^* vs. the enthalpy flux scaling parameter $\pi_4 = C_m\sqrt{RT_0/gD}$. Note that C_m is actually not constant, but for given drywell conditions depends on the dimensionless pressure difference across it, $(P_0 - P)/P_0$ (Fig. 6). We have chosen the value of C_m at $(P_0 - P)/P_0 = 1/3$ as a reference value, and it is that value which is used in the abscissa in Fig. 5 and subsequent figures.

It is clear from Fig. 5 that at the same values of π_4 (and π_1, π_2, and π_3, which are the same for all points shown)--but with different orifices d_i/d --the tests with helium and argon do have the same dimensionless pressures (to within ±10% or so, which is consistent with the experimental reproducibility). Similar results are obtained for other values of P_0/P_i and $P_i/\rho gD$. In other words, Moody's scaling laws are supported.

Figure 7a shows the three times, in dimensionless form $t^* \equiv t\sqrt{g/D}$, corresponding to the data in Fig. 5. Again, it is clear that t^* is a function of the four dimensionless scaling parameters π_1 to π_4, and Moody's scaling laws are supported. (Actually, none of the times are very sensitive to π_4, or to d_i/d, in this instance, and hence the case for the enthalpy flux parameter π_4 is made more by Fig. 5

vs. Fig. 6 rather than by comparison of the times.)

Figures 8 and 9 show a typical comparison of the dimensionless pressure obtained with air/water in the medium system (D = 28 cm) and the small system (D = 14 cm). Again, the comparison favors Moody's scaling laws, where the enthalpy flux parameter π_4 must be simulated by using out-of-scale orifices. The case made by these data is somewhat weaker than the helium-argon comparison, mainly because the differences in p^* brought about by a factor of two change in scale alone are not that great. With identically structured downcomers (same d_i/d), the p^* for the minimum floor pressure differ by about a factor of two. The ceiling pressures actually seem to scale as well as by Moody's scaling laws (c.f. Figs. 8 and 9). This is a fluke, however. In other data, the ceiling pressures do not scale at the same d_i/d. The scaling with Moody's parameters is, on the average, distinctly and consistently superior. Comparison of the dimensionless times for the small and medium systems are shown in Fig. 7b.

4.3 Peak Floor Pressures After Vent Clearing: Role of Fluid Structure Interactions

The oscillations which are set up in our test section immediately after vent clearing (Fig. 3a) appear to be at least partly due to structural vibrations caused by the almost impulsive loading of the wetwell floor and walls at the instant that the downcomer clears. That structural vibrations play a role is evident from the fact that the floor pressure oscillations can be affected by the type of structure used to support the floor and walls of the wetwell. We outline here some of

our experimental observations as they relate to this problem and present a qualitative description of a possible mechanism for the fluid-structure interaction.

The floor pressure trace shown in Fig. 3a was taken with the bottom of the medium system test section resting flush on some flat, 1" thick steel plates, and the test section clamped down from the top onto the plates. In contrast, Fig. 10a shows a trace taken when the test section was clamped down on a metal ring instead, so that the test section floor had more freedom to vibrate, while Fig. 10b shows the floor pressure when the test section rested on some strips of plasticene, and was not clamped down from the top. (Figures 3a, 10a, and 10b should not be compared quantitatively, since the test conditions were not absolutely identical, though they were roughly similar.) It is evident that the post-clearing oscillation has been changed significantly by these changes in system support structure. The frequencies observed in the post-clearing pressure oscillations are of the same order as the floor pressure oscillation frequencies produced when the (water-filled) test section was tapped with a mallet.

Quite similar results were obtained in the small system (D = 14 cm): post-clearing oscillations were observed, the frequency was of the order of the structural response frequency, and the amplitude of the oscillations and their decay rate seemed to be affected by how the test section was mounted and held.

Two points emerge from these results: (a) the post-clearing oscillations are clearly affected by conditions external to the hydrodynamics,

and (b) the frequencies observed appear to be those associated with structural response. Clearly, Moody's scaling laws cannot be expected to apply to the post-clearing oscillations. They were derived on the assumption of perfectly rigid, immobile wetwell walls.

The post-clearing floor pressure oscillations appear to be associated with structural vibrations which result from the suddenly applied load. Prior to downcomer clearing, our experimental pressure traces reveal that almost the entire pressure drop P_o-P_i occurs across the accelerating liquid slug in the downcomer, with little effect on the floor pressure. As soon as the downcomer clears, however, the liquid below the downcomer outlet is suddenly exposed to the higher pressure in the downcomer. Thus the floor pressure tends to change almost as a step function from P_i (plus the small hydrostatic change in the pool) to the instantaneous pressure in the downcomer. This sudden loading results in a small deflection of the wetwell floor and walls. Because of the inertia associated with the liquid pool and the structure itself, there is an overshoot in the deflection and subsequent oscillation. Although the deflections are very small, the pool accelerations which result from the sympathetic pool vibration are not small, because of the relatively high vibrational frequencies. Thus the vibration-induced pressure fluctuations in the liquid pool can be of significant magnitude. In contrast, the ceiling pressure histories are unaffected by the vibration (Fig. 3c and the bottom trace in Figs. 10a and 10b) because of the much smaller inertia of the fluid (air) adjacent to the ceiling-mounted transducer. A simple analysis shows that while the

frequency of oscillation does depend on system strcture, the vibration-induced pressure fluctuations are independent of system stiffness, and are typically of the same order as the pressure step that gives rise to the original deflection (P_0-P_i).

Not all of the "fine structure" on the post-clearing floor history can be attributed to structural oscillations. The prominent N-shaped portion which in Fig. 3a occurs at about 40 ms is certainly due to a hydrodynamic effect (probably a temporary occlusion of the downcomer mouth) since it shows up also on the pressure in the air in the downcomer. Furthermore, there does appear to be a correlation between the frequencies of the later post-clearing oscillations and hydrodynamic parameters. At this time we conclude only that fluid-structure interaction definitely can have a significant effect on post-clearing floor pressures.

One notes that post-clearing oscillations in floor pressure (i.e., pressure on submerged parts of the wetwell wall) were observed in GE's scale-model tests of the Mark I containment system, both in the 1/12-scale model [2] as well as the 1/4-scale model [3] tested more recently. In their 1/12-scale model studies, GE found an unexplained difference between the peak floor loads (which occur during the post-clearing oscillations) measured in their December 1975 test series and those measured in the January 1976 test series, and noted that the only difference between the two series was the grouting of the basemat on which the test cell stood. A difference in structural oscillations due to a change in grouting is consistent with many of our own tests, where we have seen differences brought about by such things as simply lightly

greasing the bottom of the wetwell before mounting it.

Pressure oscillations due to structural response vibrations will be present whenever the period of the structural vibrations (with water in the wetwell) is not small compared with the time span associated with the sudden application of the pressure load at vent clearing. This is true in our models, and also in the models used by GE for their Mark I system testing. Even more to the point, it is generally expected to be true for full-scale containment systems. In short, the peak floor pressure which occurs just after vent clearing may be expected to depend on structural as well as hydrodynamic considerations.

It should be emphasized that if the amplitudes of the deflections of the structure are very small compared with the system size we would not expect pool displacements, pool swell velocities or pressures in the wetwell or downcomer airspaces to be significantly affected by the fluid-structure interaction. Our experimental data support this conclusion. Only the pressures on the submerged walls of the wetwell, measured immediately after downcomer clearing (before structure vibration has been damped out) are clearly sensitive to structure vibration.

5. CONCLUSIONS

Based on the results we have obtained so far, our conclusions are the following:

1. The floor pressure history immediately after vent clearing in our system carries an oscillating component which appears to be affected by fluid-structure interactions, and hence may not scale accurately with Moody's scaling laws. The period involved is, however, a short one in the blowdown process.

2. After the fluid-structure oscillations have decayed, floor pressure history scales with Moody's laws to a good approximation, both as regards pressure magnitude and time, up to pool breakthrough. Also, the ceiling pressure in the wetwell (i.e., the pressure in the airspace) scales, to a good approximation, according to Moody's laws throughout the entire blowdown history, up to pool breakthrough. In order to obtain proper scaling, it is necessary to adjust the enthalpy flux in the downcomer by using orifices so that the enthalpy flux scaling parameter π_4 is properly simulated. If the gas scaling parameter π_1 and the pressure scaling parameters π_2 and π_3 are simulated, but π_4 is not (as would occur, for example, when out-of-scale orifices are not introduced), the pressure scaling can be significantly off.

REFERENCES

1. F.J. Moody, unpublished GE reports, 1975 and 1976. See summary in Reference 2 below.
2. J.E. Torbeck, D.L. Galyardt, and J.P. Walker, "Mark I 1/12-Scale Pressure Suppression Pool Swell Tests," GE Report NEDE-13456, March 1976.
3. Private communication from GE.

TABLE 2. Values of Dynamic Scaling Parameters

Parameter	Mark I System	MIT System (Design Conditions)
γ	1.4	1.4, 1.67
$\frac{P_i}{\rho g D}$	2 - 3 †	4.2, 8.4
P_o/P_i	1 - 3	2.0, 2.5, 3
$C_m \left(\frac{RT_o}{gD}\right)^{\frac{1}{2}}$	c:a 25 †	5 - 50

---

†For the Mark I system, we take

$$D^2 \equiv \frac{4}{\pi} \text{(pool area per downcomer)} \quad .$$

TABLE 1. Geometric Parameters of MIT Wetwell System

$\frac{\text{downcomer area}}{\text{pool area}}$	= 0.033
$\frac{\text{submergence}}{\text{downcomer diameter}}$	= 2
$\frac{\text{liquid depth}}{\text{downcomer diameter}}$	= 6
$\frac{\text{wetwell gas volume}}{\text{liquid volume}}$	= 1

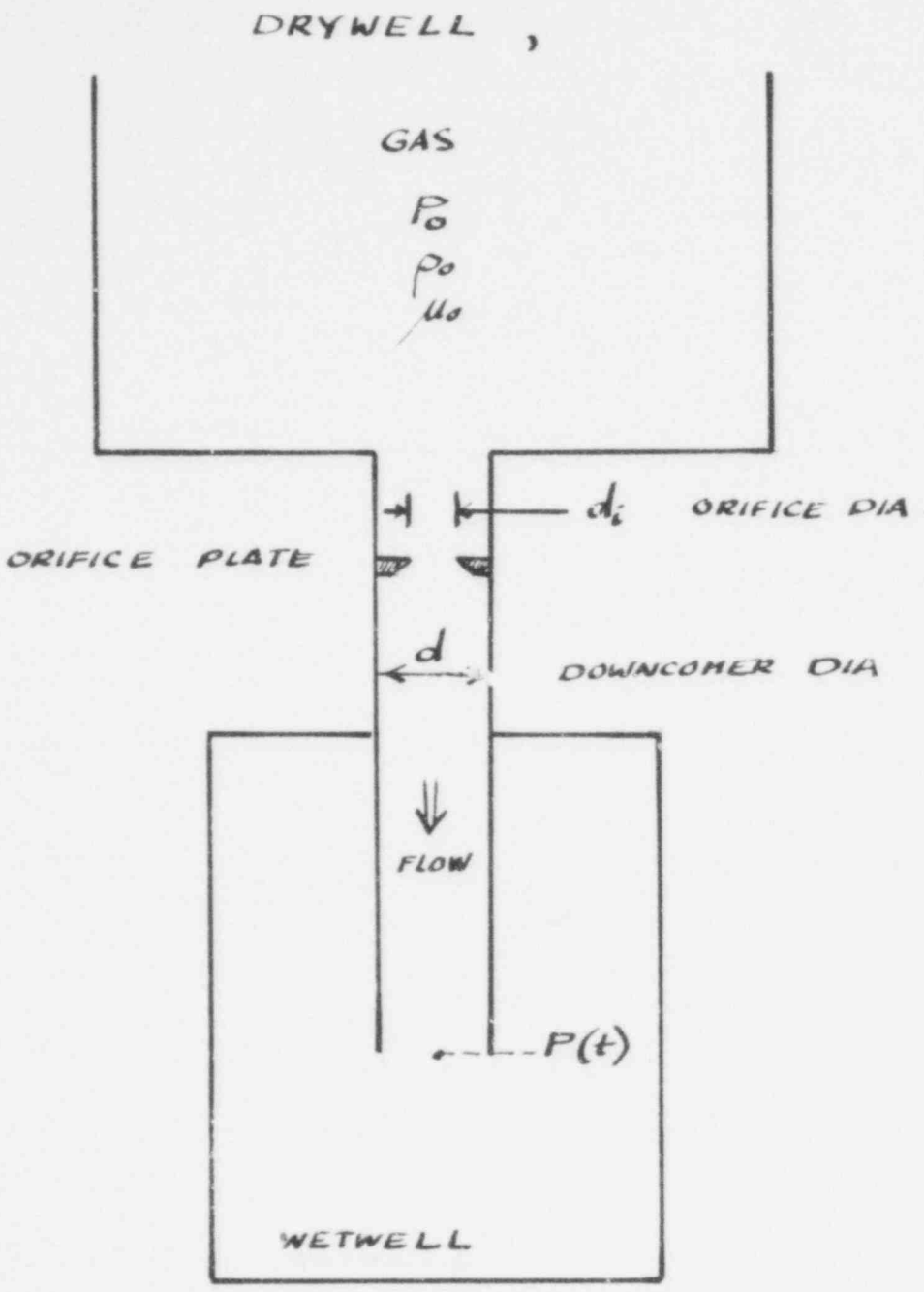

FIG. 1 : SKETCH FOR DERIVING SCALING LAWS FOR GAS FLOW THROUGH ORIFICED DOWNCOMER

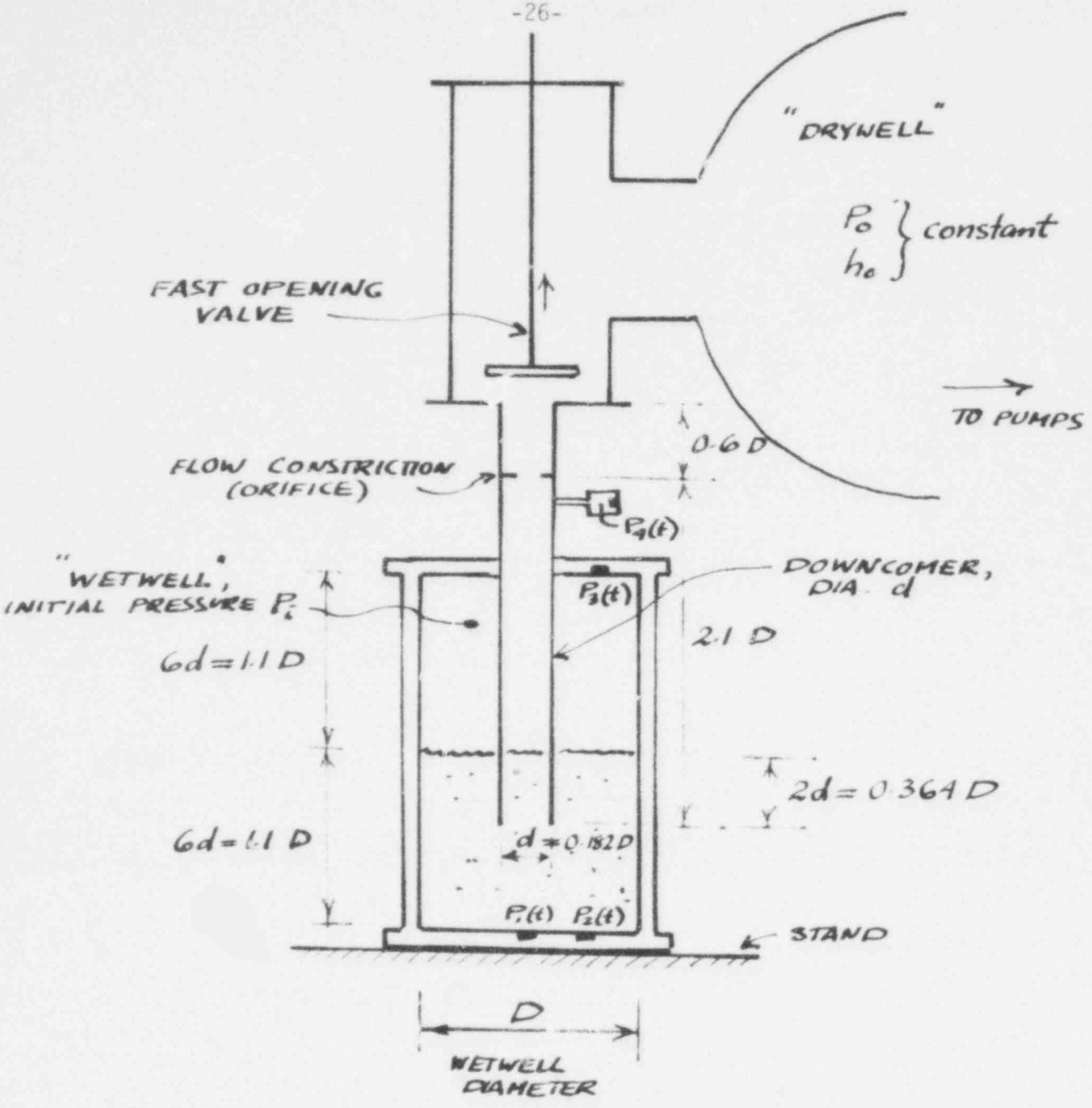

FIG. 2: SKETCH OF MIT TEST FACILITY, SHOWING WETWELL GEOMETRY AND LOCATIONS OF PRESSURE TRANSDUCERS $P_1(t)$ TO $P_4(t)$.

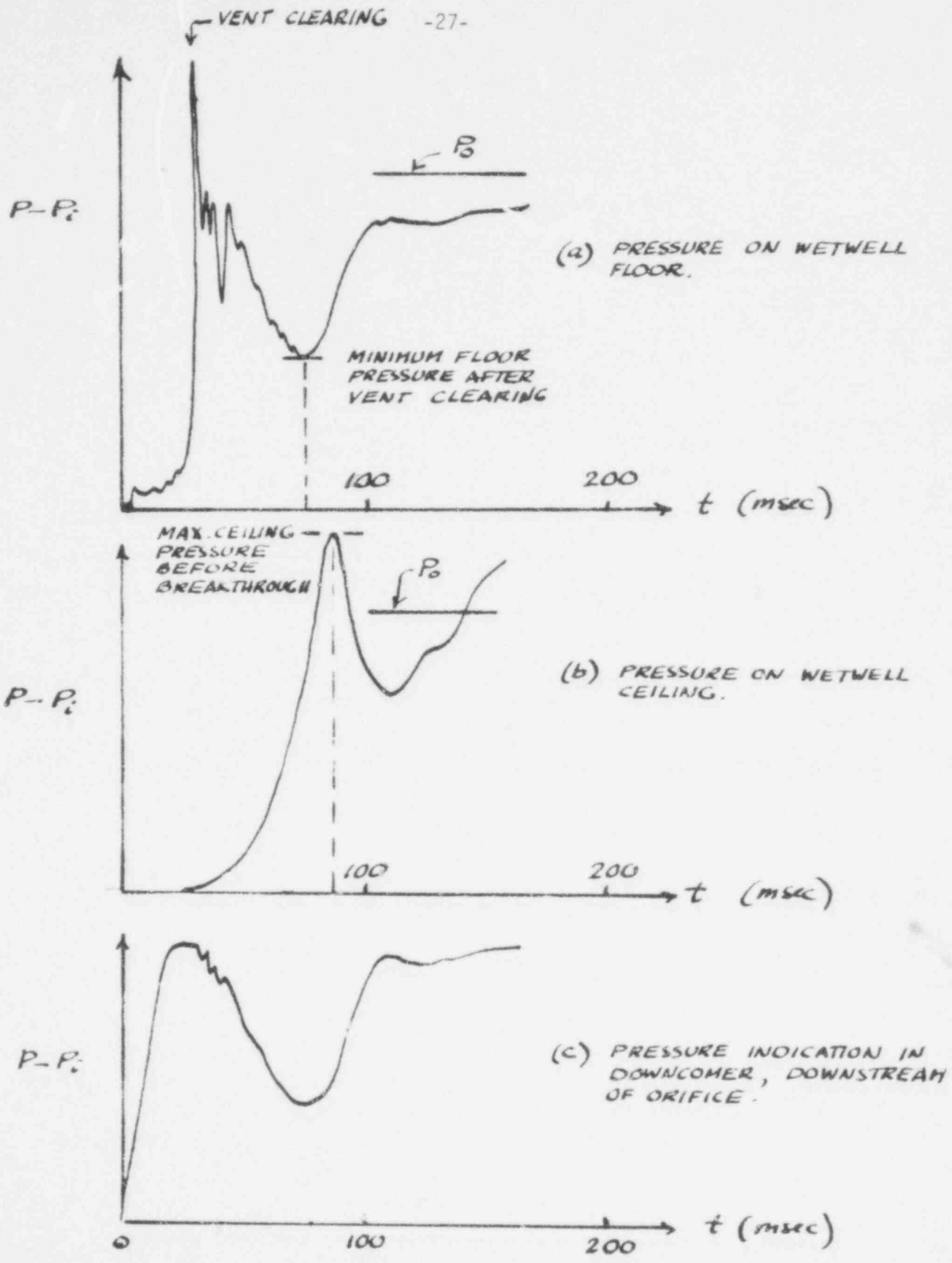

FIG. 3 : PRESSURE HISTORIES MEASURED IN MEDIUM-SIZE SYSTEM. HELIUM/WATER ; $P_i = 85$ torr ; $P_o = 255$ torr. $d_i/d = 0.470$.

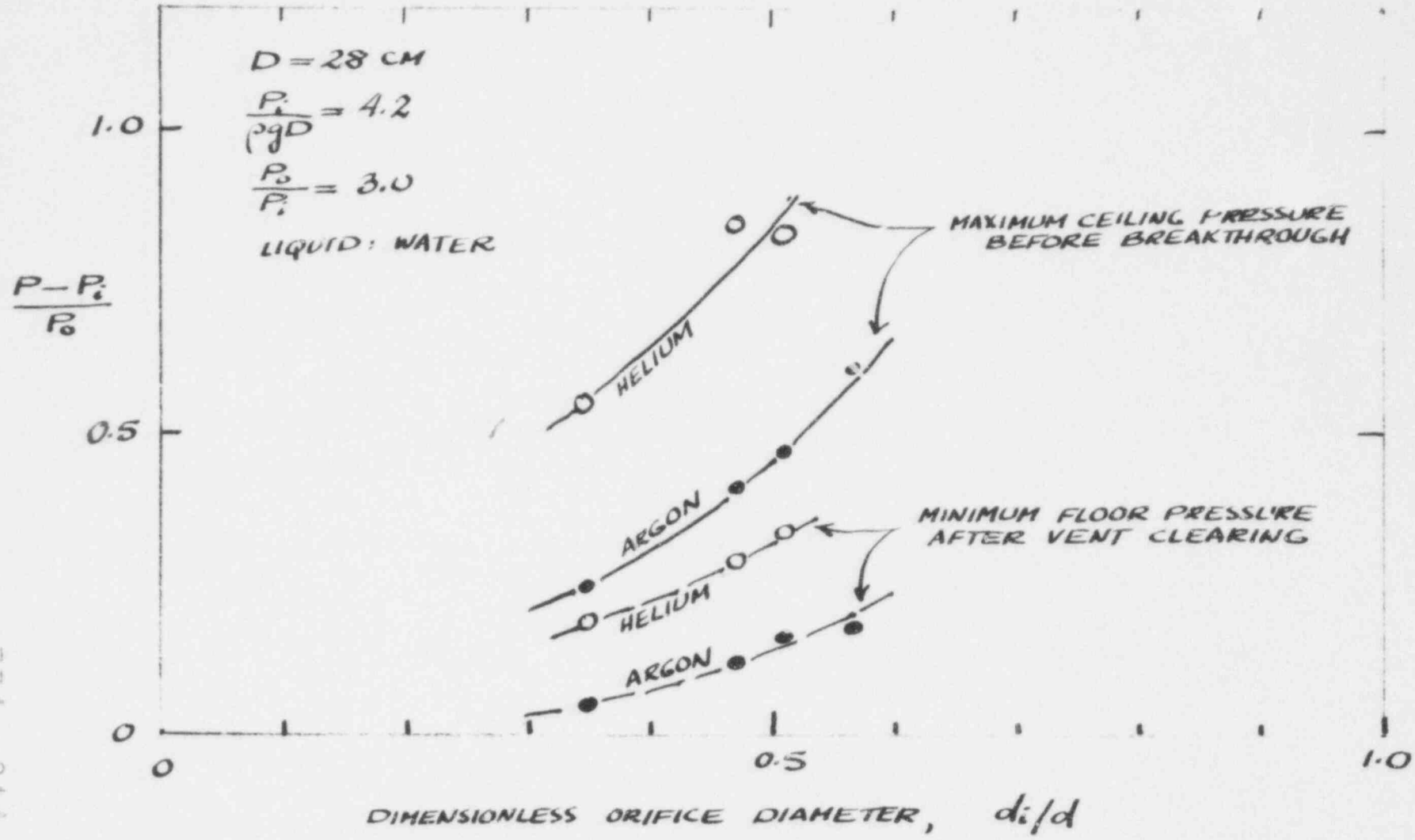

FIG. 4 : DIMENSIONLESS PRESSURES VERSUS DIMENSIONLESS ORIFICE DIAMETER FOR HELIUM AND ARGON IN MEDIUM SYSTEM.

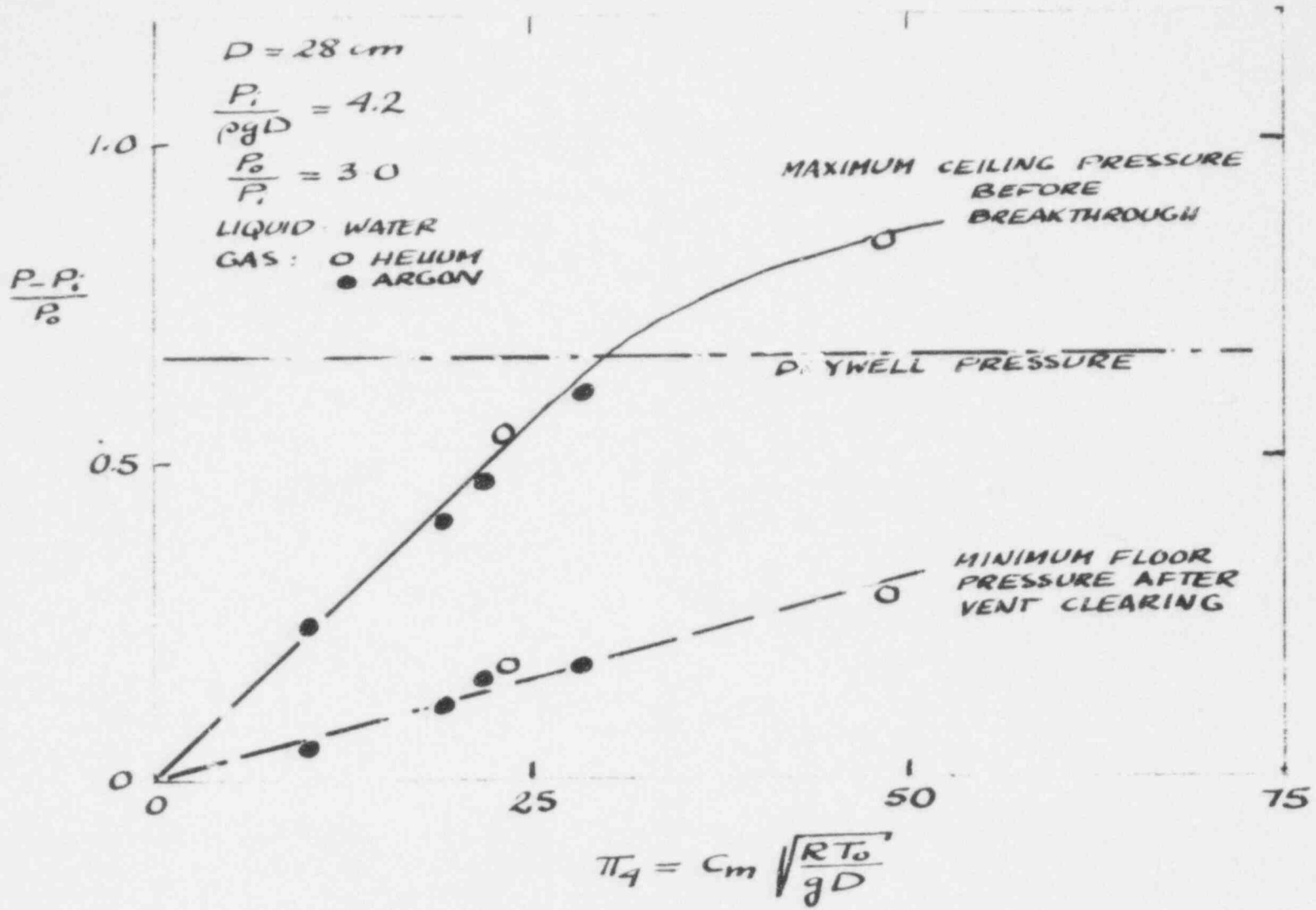

FIG. 5 : DIMENSIONLESS PRESSURES VERSUS π_4 FOR HELIUM AND ARGON IN MEDIUM SYSTEM.

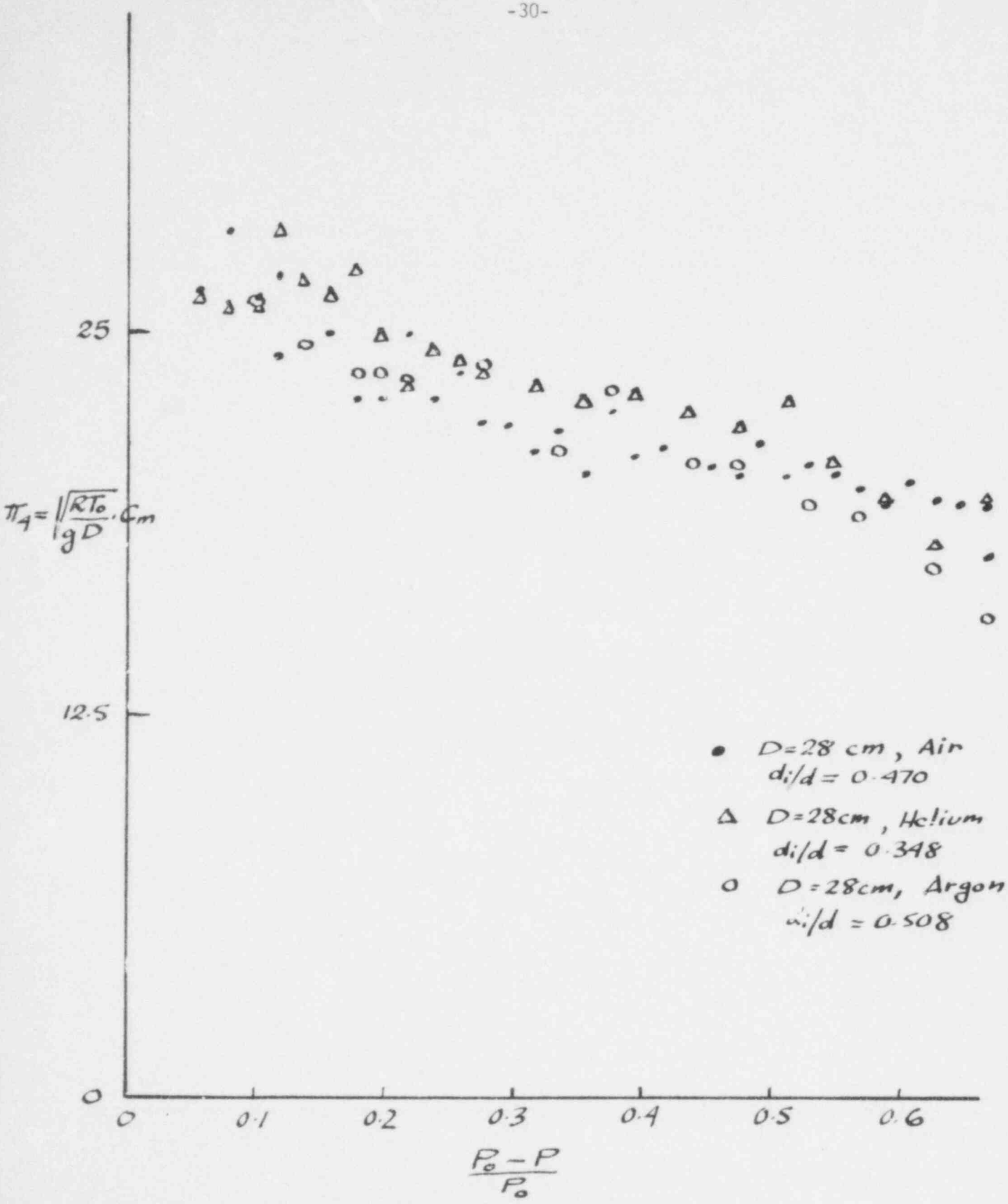

FIG. 6 : THREE ORIFICE CALIBRATIONS.

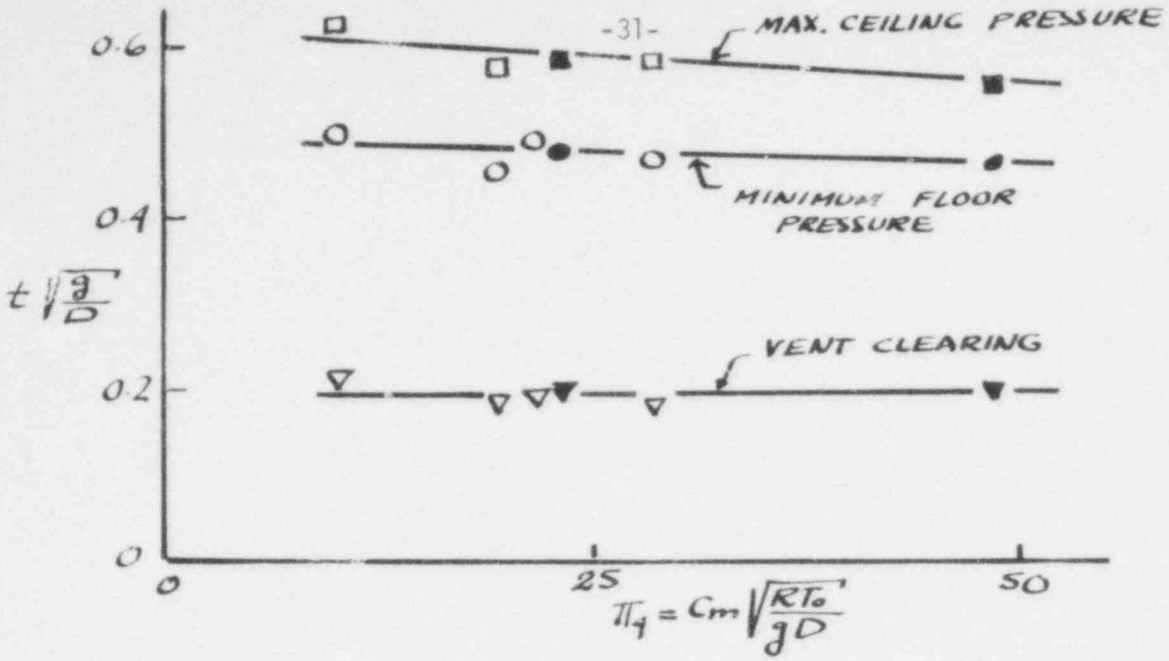

(a) MEDIUM SYSTEM ($D = 28$ CM) : ▽□○ ARGON / WATER
▼■● HELIUM / WATER

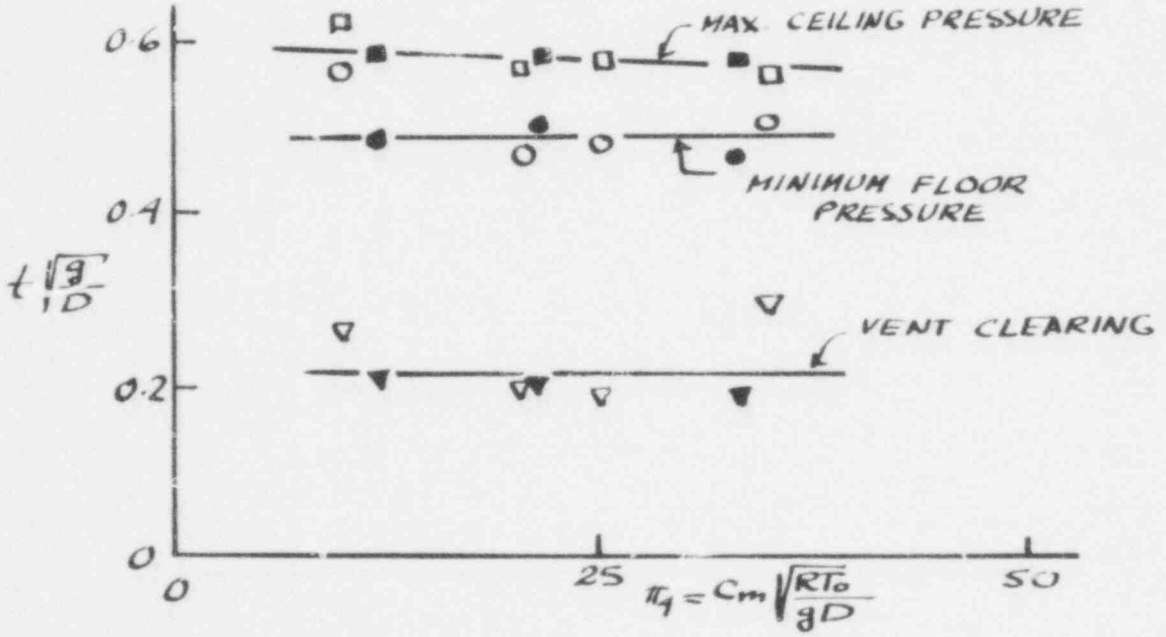

(b) AIR/WATER TESTS : ▽□○ — SMALL SYSTEM ($D = 14$CM)
▼■● — MEDIUM SYSTEM ($D = 28$CM)

FIG. 7 : DIMENSIONLESS TIMES V.S. π_4, FOR THE CASE $P_i/\rho gD = 4.2$, $P_o/P_i = 3$.

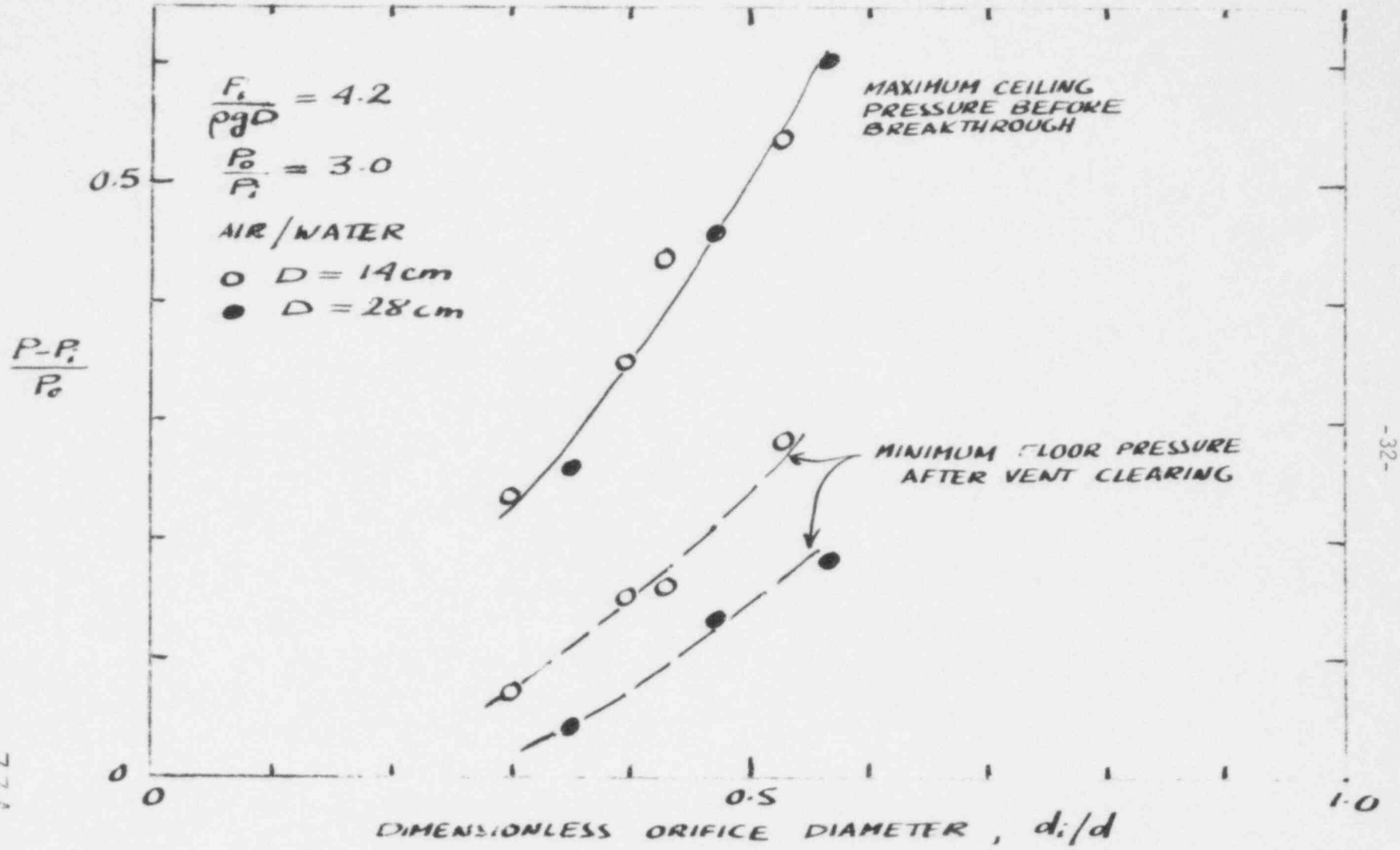

FIG. 8 : COMPARISONS OF SMALL AND MEDIUM SYSTEM PRESSURES WITH GEOMETRICALLY SIMILAR ORIFICES.

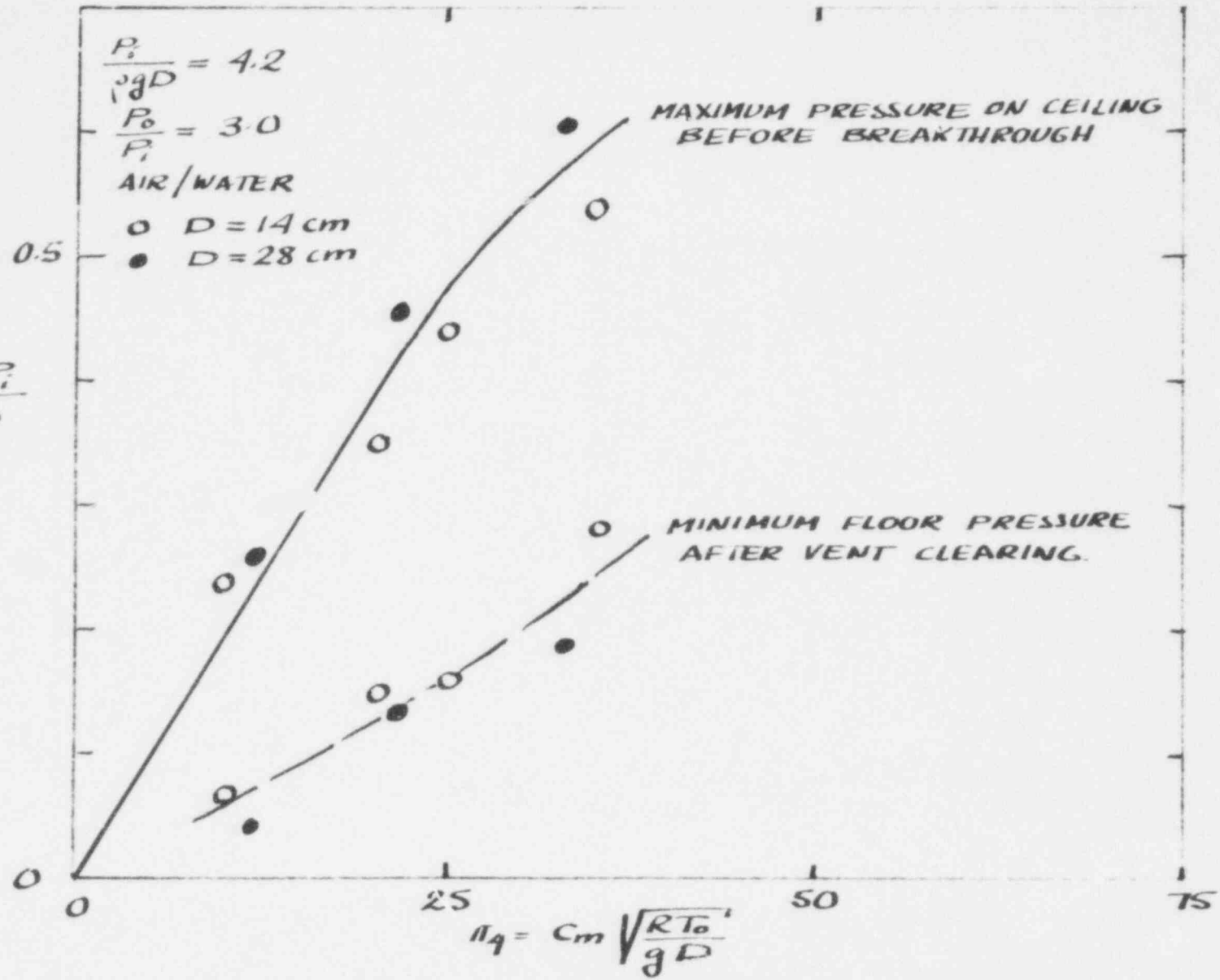

FIG. 9: COMPARISON OF SMALL AND MEDIUM SYSTEM PRESSURES AT SAME VALUES OF Π_1 TO Π_4.

(a)

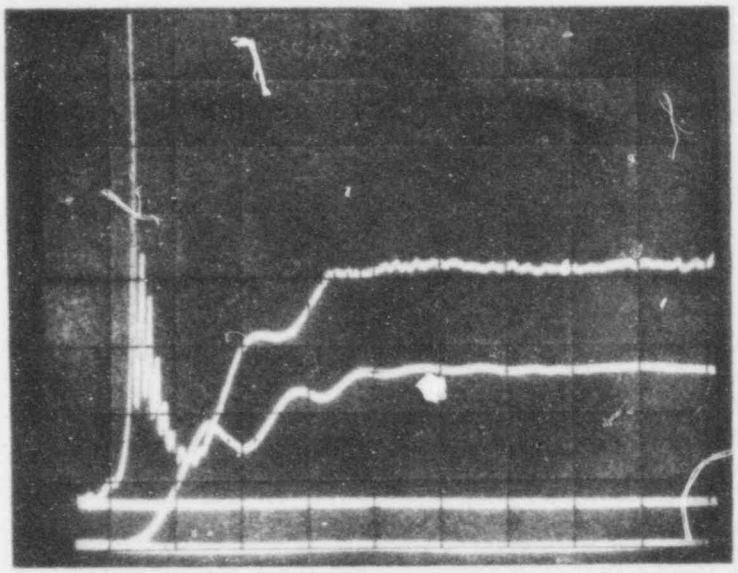

(b)

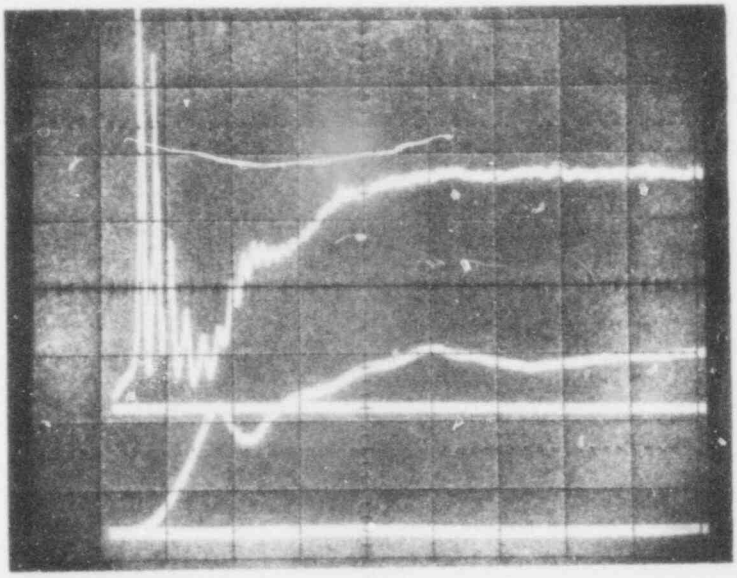

FIG. 10 : PRESSURE HISTORIES WITH (a) MEDIUM SYSTEM CLAMPED DOWN ON A METAL RING AND (b) RESTING ON PLASTICINE STRIPS.

TOP TRACES: FLOOR PRESSURE

BOTTOM TRACES: CEILING PRESSURE

HORIZONTAL SCALE: 50 msec/division

UNITED STATES
NUCLEAR REGULATORY COMMISSION
WASHINGTON, D. C. 20555